Title

Intracellular oxygen mapping using a myoglobin-mCherry probe with fluorescence lifetime imaging.

Journal

Journal of Biomedical Optics, 23(10)

Authors

Penjweini, Rozhin
Andreoni, Alessio
Rosales, Tilman
et al.

Publication Date

2018-10-01

DOI

10.1117/1.JBO.23.10.107001

Peer reviewed

Journal of Biomedical Optics

BiomedicalOptics.SPIEDigitalLibrary.org

Intracellular oxygen mapping using a myoglobin-mCherry probe with fluorescence lifetime imaging

Rozhin Penjweini
Alessio Andreoni
Tilman Rosales
Jeonghan Kim
Michael D. Brenner
Dan L. Sackett
Jay H. Chung
Jay R. Knutson

SPIE.

Rozhin Penjweini, Alessio Andreoni, Tilman Rosales, Jeonghan Kim, Michael D. Brenner, Dan L. Sackett, Jay H. Chung, Jay R. Knutson, "Intracellular oxygen mapping using a myoglobin-mCherry probe with fluorescence lifetime imaging," *J. Biomed. Opt.* **23**(10), 107001 (2018), doi: 10.1117/1.JBO.23.10.107001.

Journal of Biomedical Optics 23(10), 107001 (October 2018)

Intracellular oxygen mapping using a myoglobin-mCherry probe with fluorescence lifetime imaging

Rozhin Penjweini,[a] Alessio Andreoni,[a] Tilman Rosales,[a] Jeonghan Kim,[b] Michael D. Brenner,[a] Dan L. Sackett,[c] Jay H. Chung,[b] and Jay R. Knutson[a,*]

[a]National Heart, Lung, and Blood Institute, National Institutes of Health, Laboratory of Advanced Microscopy and Biophotonics, Bethesda, Maryland, United States

[b]National Heart, Lung, and Blood Institute, National Institutes of Health, Laboratory of Obesity and Aging Research, Bethesda, Maryland, United States

[c]Eunice Kennedy Shriver National Institute of Child Health and Human Development, National Institutes of Health, Cytoskeletal Dynamics Group, Division of Basic and Translational Biophysics, Bethesda, Maryland, United States

Abstract. Oxygen (O_2) is one of the most important biometabolites. In abundance, it serves as the limiting terminus of aerobic respiratory chains in the mitochondria of higher organisms; in deficit, it is a potent determinant of development and regulation of other physiological and therapeutic processes. Most knowledge on intracellular and interstitial concentration ($[O_2]$) is derived from mitochondria isolated from cells or tissue biopsies, providing detailed but nonnative insight into respiratory chain function. The possible loss of essential metabolites during isolation and disruption of the normal interactions of the organelle with the cytoskeleton may cause these data to misrepresent intact cells. Several optical methodologies were also developed, but they are often unable to detect heterogeneity of metabolic characteristics among different individual cells in the same culture, and most cannot detect heterogeneous consumption within different areas of a single cell. Here, we propose a noninvasive and highly sensitive fluorescence lifetime microscopy probe, myoglobin-mCherry, appropriate to intracellular targeting. Using our probe, we monitor mitochondrial contributions to O_2 consumption in A549 nonsmall cell lung cancer cells and we reveal heterogeneous $[O_2]$ within the intracellular environments. The mitochondrial $[O_2]$ at a single-cell level is also mapped by adding a peptide to target the probe to the mitochondria. [DOI: 10.1117/1.JBO.23.10.107001]

Keywords: intracellular oxygenation; mitochondria; Myo-mCherry; mtMyo-mCherry; fluorescence lifetime microscopy.

Paper 180404R received Jul. 3, 2018; accepted for publication Sep. 4, 2018; published online Oct. 8, 2018.

1 Introduction

Oxygen (O_2) and its reduced products are essential for mitochondrial functions: maintaining appropriate redox balance, numerous enzymatic reactions, cell signaling, and energy production.[1,2] The oxygen concentration ($[O_2]$) dynamically changes due to any imbalance in consumption and supply in response to the microenvironment and cellular activity. Cells have developed metabolic, transcriptional, and systemic responses to alterations in O_2 demand or supply directed toward survival and protection to cope with such threats.[2] However, long-term alterations in $[O_2]$ due to many (patho)physiological conditions, including age-related pathologies, ischemia/stroke, type 2 diabetes mellitus, excitotoxicity, neurodegeneration, cancer, inflammation, and brain injuries induce mitochondrial dysfunction, energy crisis and cell death.[2,3] Therefore, monitoring of the intracellular $[O_2]$ consumption and heterogeneity can provide a marker for the state of cellular metabolism, or track the effects of different drug treatments on cell metabolism related to disease states.[2,4,5]

As mitochondria are the primary consumers of O_2 in cells (to allow oxidative phosphorylation),[6] most knowledge on cellular $[O_2]$ level is derived from isolated mitochondria from cells or tissue biopsies, and these studies provided detailed insights into respiratory chain function. However, the O_2 dependence of mitochondrial and cellular respiration has remained controversial because the literature contains some conflicting results and conclusions.[3,7,8] The apparent conflicts might be reconciled if the limitations of the methods and techniques used are taken into account. For example, the possible loss of essential metabolites during mitochondrial isolation and disruption of the organelle regulation (e.g., morphology and directed/diffusive motion)—along with normal interactions with the cytoskeleton—may cause these data to misrepresent the metabolic conditions of intact cells and tissue.

Because of the critical need to measure $[O_2]$ levels and consumption in intact tissue, MRI imaging and several optical methods were developed.[9,10] The indirect assessment of $[O_2]$ in MRI imaging has huge clinical impact, with great penetration but millimeter resolution.[11] Optical assessment of $[O_2]$ with exquisite submicron resolution is limited by the attenuation and scattering properties of tissue to a few millimeters depth, unless one is willing to work in the photon diffusion regime where a few centimeters depth inevitably degrades resolution to several millimeters. Moreover, many of these methods are dependent on injection of an organic compound or insertion of a needle or catheter into the desired location that may result in cytotoxicity, inflammation, injury to the tissue, and artifacts in the measurements.[12]

*Address all correspondence to: Jay R. Knutson, E-mail: knutsonj@nhlbi.nih.gov

1083-3668/2018/$25.00

The primary means of detecting $[O_2]$ in the microscope have been either photoacoustic (point measurements with a few microns resolution) or phosphorescent. The latter relies on the Stern–Volmer quenching of a luminophore by collision, and the 10 s to 100 s of microseconds between such collisions are in reach of the phosphors lifetimes (τ_p).[9] Unfortunately, natural phosphors of porphyrin parentage are disruptive in cells and exogenous phosphors are difficult to target to cell interiors.[13] Nevertheless, much useful information is gleaned from point measurement of phosphorescence lifetime. The limitation to a few points rather than full-field scans is due to the requirement that one dwell on at least a few multiples of the τ_p before departing a voxel. Moreover, due to the long lifetime and concomitant low yield of phosphorescence probes, an accurate measurement of $[O_2]$ based on phosphorescence lifetime imaging (PLIM) requires long acquisition time. Due to the motions and dynamic rearrangements often observed in live cells and tissue at the subcellular level, or body motion and even the heartbeat of the animals during imaging, long acquisition time is a practical problem for live-cell imaging and *in vivo* studies. Optical assessment of $[O_2]$ using phosphorescence intensity alone can also be misleading because the concentration of phosphorescent dye and/or intensity of the excitation light are different in different regions inside a cell or tissue.[9,12,14,15]

We sought to instead develop a fluorescence lifetime microscopy (FLIM) probe appropriate to intracellular targeting. Inspired by Thompson's use of protein Zn^{2+} sensors coupled to fluorophores,[16] we sought to couple a reporter fluor to the natural $[O_2]$ binding protein myoglobin. At first, we read out the $[O_2]$ occupancy with red fluorescent dyes (e.g., Alexa594) *in vitro* (data have not been published), then we developed a Förster resonance energy transfer (FRET)-based O_2 probe, myoglobin-mCherry (Myo-mCherry). In this study, we used a unique combination of Myo-mCherry probe with two-photon FLIM, to noninvasively and accurately monitor the intracellular $[O_2]$ and heterogeneity in living A549 nonsmall cell lung carcinoma culture. To measure the mitochondrial contribution to intracellular O_2 consumption, $[O_2]$ level in A549 cells in response to external $[O_2]$ variation was compared to those in A549 mitochondrial DNA-depleted (mtDNA) ρ^0 counterparts that are incapable of aerobic respiration due to the lack of key respiratory chain components. Further, any intracellular heterogeneity of mitochondrial $[O_2]$ was probed within living cells by adding a peptide to direct Myo-mCherry (via the mitochondrial-targeting sequence), a targeting that would be difficult, if not impossible, to study with aforementioned techniques. The O_2 sensing method proposed in this study has several advantages over the existing optical methods: (i) mCherry is known as a biocompatible protein,[17–19] and Myo-mCherry can be expressed in the cells without showing clear signs of cytotoxicity, with cells surviving even 3 days after transfection. (ii) $[O_2]$ obtained based on FLIM-FRET measurements are independent of Myo-mCherry dose, heterogeneity, and fluorescence intensity. (iii) mCherry has a short lifetime in the intracellular environment (~1.34 to 1.36 ns) and reasonable quantum yield (QY); although mCherry has been reported to have two intrinsic lifetimes,[20] and hetero-FRET between mCherry molecules may play a role in FLIM, our control measurements (lifetime imaging of the cells transfected with only mCherry) suggest that hetero-FRET does not occur in the concentration range used in our experiments. (iv) Myo-mCherry can target mitochondria to measure their oxygenation level. (v) To ascertain whether $[O_2]$ is experiencing large gradients in and around various organelles, we can target either Myo-mCherry or control mCherry to those sites to look for any microenvironment sensitivity.

2 Working Principle of the Myo-mCherry Probe

Myo-mCherry is a FRET-based probe that was constructed by expressing in tandem myoglobin and the red fluorescent protein mCherry [Fig. 1(a)]. The absorption spectrum of myoglobin in the 550 to 700 nm region overlaps with the emission of mCherry [Fig. 1(b)], resonance energy transfer can thus occur between the red fluorescent protein (donor) and myoglobin (nonfluorescent acceptor). The spectrum of myoglobin changes upon binding and unbinding of O_2. Therefore, the spectral overlap varies in an O_2 dependent manner [Fig. 1(b), shaded area]: when O_2 is bound (left panel), mCherry's fluorescence will only be marginally quenched, and when O_2 is released the energy transfer will increase (right panel). Thus, when the probe is deoxygenated (deoxy), the emission intensity and correspondingly the lifetime will decrease compared to the oxygenated (oxy) form. It is important to notice that the FRET probe presented here is not based on distance changes between the two partners, but solely on changes in the spectral features of the energy acceptor. The Förster radius (R_0) between mCherry and myoglobin, calculated based on the spectral features, changes upon oxygenation and deoxygenation; this leads to a change in the energy transfer function, as shown in Fig. 1(c). The distance between the two proteins is defined by the linker that connects them. Although no structural data for the construct are available, by using the protein data bank (PDB) deposited structures of each protein, it is possible to approximately estimate a distance of ~4 nm between the two chromophores [dashed line, Fig. 1(c)]. Furthermore, using the published spectral data for myoglobin and mCherry,[21,22] and the reported extinction coefficients of the two proteins,[23] it is possible to (approximately) estimate R_0 for the oxy and deoxy form of the construct. Although biophysical characterization of the probe goes beyond the scope of this paper, more detailed calculations on the presented FRET system are provided in Appendix.

Since the intensity of Myo-mCherry images are dependent on both an unknown concentration and the degree of FRET, we instead chose fluorescence lifetime imaging (nearly concentration independent), achieved through two-photon excitation, to reveal FRET rate and therefore (de)oxygenation level of the probe. The two-photon excitation of mCherry at 780 nm is not blocked by inner filter from the Q-band absorption of myoglobin, since its absorbance at this wavelength is negligible. Note further, even though excitation of the heme by stimulation of Soret band (~390 nm) is possible via a two-photon process, the excited state of the cofactor has a duration of only a few picoseconds (ps),[24] and myoglobin is essentially nonfluorescent on its own.

We estimate that the intracellular concentration of Myo-mCherry in our work is on the order of micromolar to submicromolar, and we did not image cells showing unusually high fluorescence to avoid intermolecular FRET. Based on our calculations, the Förster radius between mCherry and myoglobin is ~4 nm. For efficient FRET to occur, the two proteins would have to be close-almost in contact, hence our choice of using a very short linker between the two. To achieve intermolecular FRET, either K_D in the micromolar range would be needed, or if

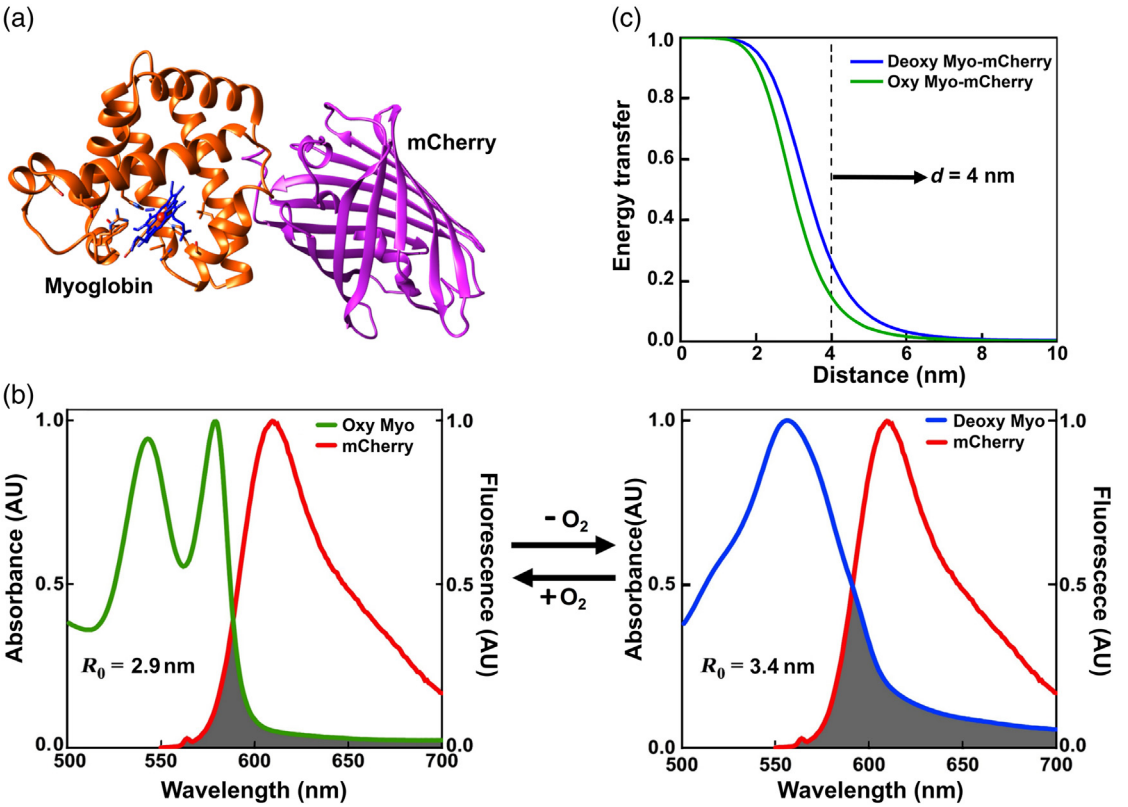

Fig. 1 (a) Artist's rendering of the Myo-mCherry construct, where mCherry (PDB: 2H5Q) was coupled to the C-terminus of myoglobin (PDB: 1MBO). (b) Absorption spectra[22] of oxygenated (oxy) and deoxygenated (deoxy) myoglobin, in green and blue, respectively, overlapped with the emission spectrum of mCherry, in red, to highlight the spectral overlap (shaded area) between the species. R_0 is the Förster radius calculated based on the spectral data shown here. (c) Energy transfer for the Myo-mCherry system as a function of distance between the two proteins. The dashed line at 4 nm highlights the average distance between the two proteins as inferred from the available structures and data of the individual component [21–23] (See Appendix for more details on the calculations).

truly random, the intracellular concentration of our probe would have to be such that the distance between chromophores would be on the order of ~3 nm or less.[25] Considering that in a first approximation the chromophore of mCherry is buried ~1 nm inside the protein scaffold, it can be calculated that to achieve an average ~2 nm distance between proteins the concentration should exceed a few mM. We are confident that we are working at a much lower concentration level than that. We also expect that differing levels of this transfer would interfere in the convergence of lifetime values seen at minimal oxygen levels.

3 Methods

3.1 *Preparation of Plasmid Carrying Myo-mCherry Genes and Targeting to Mitochondria*

The plasmid, pMyo-mCherry, was prepared by cloning the gene of myoglobin from *Physeter catodon* (Sperm Whale, Addgene Plasmid pMB413a, #20058)[26] into the vector pmCherry N1 (Clonetech, Mountain View, California) at the N-terminal side of mCherry. The plasmid carries a cytomegalovirus (CMV) promoter and enhancer for expression of proteins in mammalian cells. A 2-amino acid (Ser-Gly) spacer was inserted between the C-terminus of myoglobin and the N-terminus of mCherry to allow for flexibility and avoid possible misfolding that is often observed when a direct fusion of domains is attempted.[27] The pmCherry N1 plasmid was used for the expression of mCherry alone as a control.

A mitochondrial targeting sequence from human mitochondrial transcription factor A (TFAM) was added to the pMyo-mCherry vector (mtMyo-mCherry) to direct the probe to mitochondria.

3.2 *Transfection of Living Cells with Myo-mCherry*

A549 cells and their mtDNA-depleted ρ^0 counterparts were used to evaluate the efficacy of Myo-mCherry for monitoring of the intracellular and mitochondrial [O_2]. A549 human lung cancer cell lines were obtained from the National Cancer Institute (NCI) anticancer drug screen. A549 ρ^0 cells were obtained from A549 parental line by ethidium bromide selection and were the kind gift of Dr. William DeGraff, NCI. The loss of mtDNA in the A549 ρ^0 cells was confirmed by nanoString (Seattle, Washington) nCounter multiplex RNA analysis. Expression of two mitochondrial proteins, one coded by mitochondrial DNA and one by nuclear DNA, were compared in A549 and A549 ρ^0 cells. This revealed that the expression of the mitochondrially coded gene cytochrome oxidase 2 (MT-CO2, P00403) in A549 ρ^0 cells was reduced at least 10,000-fold (undetectable) compared to A549 cells. In contrast, the nuclear-coded cytochrome C1 (CYC1, P08574), was expressed in A549 ρ^0 cells at essentially the same level (1.02×) as in A549

cells. Five housekeeping proteins suggested by nanoString were expressed in A549 ρ^0 cells at essentially the same levels (average 1.1×) as in A549 cells.

A549 cells were maintained in modified eagle's medium (DMEM, Gibco, Grand Island, New York,) with 10% nonheat inactivated fetal bovine serum (Invitrogen, Grand Island, New York). The media for A549 ρ^0 was the same but supplemented with 1-mM sodium pyruvate and 5-μg/ml uridine. The cells were plated in Lab-Tek 2 well chamber (Thermo Fisher Scientific Inc., Rochester, New York) with a density of 4×10^4 cells/chamber (10^4 cells/cm^2), which provides sparse coverage of the sample chamber to prevent excessive oxygen consumption at the bottom of the culture dish. The cells were transfected according to the Lipofectamine® 2000 (Invitrogen, Van Allen Way Carlsbad, California) DNA transfection reagent protocol. Briefly, the plasmid was diluted in Opti-MEM® medium (Gibco, 2.5 μg in 125 μL) and it was added subsequently to a solution of Lipofectamine® 2000 in Opti-MEM® medium (2.5-μL lipofectamine in 25 μL medium) in a 1 : 1 ratio at room temperature. After 20 min incubation, the DNA–lipid complex was added to the cells in culture medium. The final amount of DNA and lipofectamine per well were 100 ng and 0.5 μL, respectively. After 24-h incubation with DNA–lipid complex at 37°C and 5% CO_2, the cells were washed with phosphate buffered saline (PBS, Gibco) and incubated for a further 24 h in culture medium before being imaged with a confocal two-photon laser scanning microscope. Cells transfected with plasmid, pmCherry, using the same transfection reagent and protocol were used as controls.

3.3 *Treatment of Transfected Cells with MitoTracker Green and Rotenone*

For colocalization analyses of Myo-mCherry and mtMyo-mCherry with mitochondria, A549 cells were incubated with 200-nM MitoTracker® Green (Molecular Probes®, Eugene, Oregon) for 20 min at 37°C and 5% CO_2. After labeling, the cells were washed several times by PBS and then incubated in the culture medium.

For inhibition of mitochondrial O_2 consumption, A549 cells transfected with pMyo-mCherry were treated with 500-nM rotenone for 1 h at 37°C and 5% CO_2. Different rotenone concentration and incubation times were explored to find this appropriate protocol.[28] Prolonged incubation of the cells with higher concentration of rotenone resulted in cell death. After FLIM measurements at three [O_2], a new batch of cells were incubated with rotenone using the same protocol and were used to measure at most another three responses to external [O_2]. This was to ensure the inhibition of mitochondrial O_2 consumption.

3.4 *Imaging Setup*

FLIM was performed on a commercial Zeiss LSM 510 META confocal laser scanning microscope (Zeiss, Jena, Germany) modified for two-photon excitation experiments: a solid-state CW green laser (Millennia® diode-pumped, Spectra-Physics, California) is used to pump a femtosecond pulsed titanium-sapphire oscillator (Tsunami® mode-locked, Spectra-Physics, California) operated at 80 MHz and tuned to an output wavelength of 780 nm. The infrared pulsed laser was steered into the LSM unit through a dedicated IR port and reflected by an HFT KP 700/488-nm dual band dichroic mirror onto the back aperture of a Plan-Apochromat 63×, 1.4 NA, oil immersion microscope objective (Carl Zeiss, Germany). The power was attenuated to ~8 to 12 mW, measured before the objective, for the experiments. The emission was collected through the same objective, reflected by a 735-nm long-pass dichroic mirror toward the back port of the microscope, filtered through an ET750SP-2P and an ET700SP-2P filter (750 and 700 nm short-pass, respectively, Chroma Technologies, Bellows Falls, Vermont) to remove residual scattering from the laser, and the fluorescence was further selected by a 641/75-nm band pass (BP) filter. The signal was recorded in a nondescanned detection (NDD) configuration by a H7422P-40 GaAsP photomultiplier module (Hamamatsu, Japan). The signal from the detector was directed into an SPC-150 photon counting card (Becker & Hickl, Berlin, Germany) and synchronized with the pulses from the laser, the pixel, and line clock from the confocal laser scanning unit. Images of 1024×1024 (pixels)^2 were acquired with the LSM scanner set at a pixel dwell time of 0.8 or 1.26 μs. The images were zoomed onto each cell to avoid loss of information by scanning large areas of background. While the scanner was operating in continuous mode, the FLIM images were collected by the SPC150 for times between 50 and 100 s, depending on the brightness of the selected cell. A 4-pixel divider was applied by the SPC150 acquisition software, thus the final FLIM images are 256×256 (pixels)^2: this operation still delivers optimal subresolution pixel size for the final image. The SPC150 was operated in histogramming mode to record time-correlated single-photon counting (TCSPC) histogram at each pixel with 64-time channels (0.199 ns per channel).

For colocalization analyses of Myo-mCherry and mtMyo-mCherry with mitochondria, various image series were acquired with a Zeiss LSM 780 confocal microscope (Carl Zeiss, Germany) equipped with a Plan-Apochromat $63 \times /1.4$ NA oil immersion objective. For imaging of the fluorescence of MitoTracker and mCherry, a multiline argon laser emitting at 488 nm and a diode laser emitting at 594 nm were used, respectively. The laser light was directed onto the sample using a dual-band dichroic mirror, MBS 488/594. The fluorescence collected from the sample was directed toward two photomultiplier tubes, and it was spectrally filtered by selecting a 490- to 562-nm bandpass region for the green channel, and a 603- to 721-nm bandpass region for the red channel to minimize bleed-through artifacts. The images [512×512 (pixels)^2] of each series were collected with no time delays between the sequential frames. The individual frames were acquired with a pixel size in the range of 0.05 to 0.10 μm and a pixel dwell time of 1.27 μs.

3.5 *Controlled Experimental Environment with a Range of Stable Oxygen Concentration*

To provide an environment that is nonperturbing and suitable for the homeostasis of the cells during imaging, a miniature incubator chamber (Bioscience Tools, San Diego, California) was mounted on the Zeiss microscope stage and connected to a gas mixing system ($CO_2 - O_2 -$ MI, Bioscience Tools, San Diego, California). The incubator provided temperature control, and the gas mixing system delivered preset mixtures of N_2, O_2, and CO_2 inside the chamber. The FLIM experiments were conducted at stable %O_2 (v/v) of 20%, 19%, 16%, 13%, 10%, 7%, 4%, 1%, and 0.5% in the microscope chamber; 0.5% is the lowest [O_2] obtained by our system. The environmental [O_2] was changed from atmospheric to ~0.5% step by step to avoid damage to the cells and keep them alive for long-term imaging. For O_2 depletion, experiments were conducted by blanketing the

cultures with different humidified mixtures of N_2 and O_2 with 5% CO_2 (containing ≤10 ppm O_2; AirGas) at 37°C. Our system typically allows the cell culture (in culture dishes with medium ~2 to 3 mm deep, without lids) to reach a stable $[O_2]$ within 45 min. Measurements of $[O_2]$ (in mmHg) in the cell culture media were performed in separate experiments by using a bare-fiber O_2 sensor (NX-BF/O/E, Optronix Ltd., Oxford, United Kingdom) connected to an OxyLite Pro 2 Channel monitor (Optronix Ltd., Oxford, United Kingdom). The $[O_2]$ was checked in the atmosphere inside the miniature incubator, as well as within the media at different depth, in the absence and in the presence of cells adhering at the bottom of the Lab-Tek chamber.

3.6 *Fluorescence Lifetime Analysis*

The SPCImage software (Becker & Hickl GmbH, Berlin, Germany) was used to analyze the fluorescence lifetime decay images of Myo-mCherry and mCherry at each external $[O_2]$. The decay curves at each pixel were fit to a double-exponential decay model with a minimized error of the fitting, χ^2:[20]

$$F(t) = C_1 \exp(-t/\tau_1) + C_2 \exp(-t/\tau_2), \tag{1}$$

where C_1 and C_2 are the pre-exponential factors and can be used (if natural lifetime is constant) to represent the fraction of fluorophores with lifetimes τ_1 and τ_2, respectively.

Fitting was performed via iterative reconvolution with the instrument response function (IRF), where the IRF was synthetically generated by the SPCImage software based on the rise of the experimental decay function.[29] In the presence of the FRET acceptor myoglobin, the lifetime decay of mCherry would be better described by a multiexponential function with more than two lifetime parameters (and thus more than two amplitude parameters). However, the four-parameter function in Eq. (1) adequately represents the data and can be used to glean FRET trends in terms of average lifetime. The 12.5-ns interpulse time in our laser made the "incomplete decay" model available in SPCImage unnecessary to fit for the lifetimes that we were evaluating. The typical bin value per image was 5 [which correspond to an area of 11×11 $(\text{pixels})^2$]. However, for some dimmer cells, we increased the binning to values greater than 5 to avoid using decays with a peak count lower than 1000 for two component exponential fitting. We used a threshold to avoid fitting decays with a peak count lower than 1000, and this resulted in some features apparently missing in the FLIM images. This is caused by the heterogeneous distribution of the probe in the intracellular environment, thus causing heterogeneous concentration distribution resulting in variable intensity across the cell. The shift of the IRF was determined by fitting the decay of the pixel, in each image, with the highest intensity, and it was then fixed for the calculation of the FLIM image. The offset for each pixel was determined by the software based on the tail of the decay at longer decay times. A scatter parameter was included in the fitting model: even though we used high optical density two-photon filters to remove scattered laser light and a BP filter before the detector, we cannot completely exclude that some excitation light might bleed through due to scattering from different parts of the cell (due to slight variations in refractive index, intracellular composition, and organelle arrangement). The average lifetime was calculated for each pixel via amplitude weighting, and for each image a lifetime distribution histogram was obtained. Full image averaged values of Myo-mCherry fluorescence lifetime $[\tau([O_2])]$, taken for multiple cells and loci, were correlated with $[O_2]$ (in partial pressure) by the best hyperbolic curve that was fit to the data using the Curve Fitting Toolbox in MATLAB R2016b (The MathWorks Inc., Natick, Massachusetts):

$$\tau([O_2]) = (\tau_{\max} - \tau_{\min}) \frac{[O_2]}{a + [O_2]} + \tau_{\min}, \tag{2}$$

where a is the fitting parameter and $\tau_{\max}$ and $\tau_{\min}$ are the measured lifetimes at the highest and lowest $[O_2]$, respectively. This hyperbolic equation was chosen because the probe response seems to closely resemble myoglobin oxygen dissociation behavior.[22,30] The derivation and a more detailed discussion on the significance of this equation are given in the Appendix.

3.7 *Colocalization Analyses Calculating Manders's Overlap Coefficient*

To investigate the colocalization of the Myo-mCherry and mtMyo-mCherry within the mitochondria, colocalization analyses were performed on fluorescence images of Myo-mCherry, mtMyo-mCherry, and MitoTracker green in A549 cells by using a freely available JACoP toolbox under ImageJ (National Institute of Health, Bethesda, Maryland).[31,32] For the colocalization analyses of the images A_i and B_i, Manders's coefficients M_{A-B} were defined as follows:

$$M_{A-B} = \frac{\sum_i A_{i,\text{coloc}}}{\sum_i A_i}, \tag{3}$$

where $A_{i,\text{coloc}} = A_i$ if $B_i > 0$ and $A_{i,\text{coloc}} = 0$ if $B_i = 0$.

M-values are ranging from 0 to 1, the former corresponding to nonoverlapping images and the latter reflecting absolute colocalization between both images. M-values do not depend on the instrumental amplifier setting or labeling densities.[31]

3.8 *Statistical Analyses*

For each condition, lifetime imaging was conducted for at least 20 cells. The data are presented as the mean ± standard deviation. Mann–Whitney tests were used to evaluate whether the lifetime values in each two independent groups (e.g., A549 cells, A549 mtDNA-depleted ρ^0 counterparts, A549 cells treated with rotenone, and A549 mitochondria) measured at the same external $[O_2]$ are significantly different from each other. Analyses were carried out using SPSS 14.0 (a subsidiary of IBM, Chicago, Illinois) software and statistical significance was defined at $p < 0.05$ (95% confidence level).

4 Results and Discussions

4.1 *Intracellular Colocalization of Myo-mCherry and mtMyo-mCherry with Mitochondria of A549 Cells*

Mitochondria are responsible for the majority of O_2 consumption within eukaryotes.[33] Thus, being able to target them with an O_2 probe is an important part of understanding and mapping the cellular oxygenation distribution. Herein, the subcellular localization of Myo-mCherry was analyzed and the ability to target mitochondria was checked by using mtMyo-mCherry, where a mitochondrial targeting sequence was added to the construct. Image series of A549 cells transfected either with Myo-mCherry

or mtMyo-mCherry and subsequently labeled with MitoTracker were acquired in two different emission channels: red emission of mCherry and green fluorescence of MitoTracker. The red and green channels and the overlay of the two channels are presented in Figs. 2(a)–2(c), respectively. The colocalization of Myo-mCherry or mtMyo-mCherry with MitoTracker was quantified by Manders's overlap coefficients, M.[32] $M_{\text{MitoTracker and Myo-mCherry}}$ is used to study the proportion of the mitochondria green pixels coincident with Myo-mCherry (red) pixel. The fractions of pixels related to the mtMyo-mCherry colocalized with mitoTracker are given by $M_{\text{mtMyom-Cherry and MitoTracker}}$. $M_{\text{MitoTracker and Myo-mCherry}}$ and $M_{\text{mtMyo-mCherry and MitoTracker}}$ were calculated to be 0.80 ± 0.06 and 0.90 ± 0.06, respectively. Myo-mCherry without the mitochondrial targeting sequence is not intentionally targeted to mitochondria. However, $M_{\text{MitoTracker and Myo-mCherry}}$ shows that trafficking of the protein in this particular cell line (A549), even without any targeting sequence may result in Myo-mCherry being preferentially distributed near mitochondria. Nevertheless, $M_{\text{mtMyo-mCherry and MitoTracker}}$ value near unity confirms the efficient targeting of most mitochondria in A549 cells by adding a mitochondrial targeting sequence. The transfected cells showed heterogeneous level of expression of Myo-mCherry as indicated by variation of brightness from cell to cell. However, neither bright cells nor dimmer cells showed any sign of cytotoxicity even three days after the transfection.

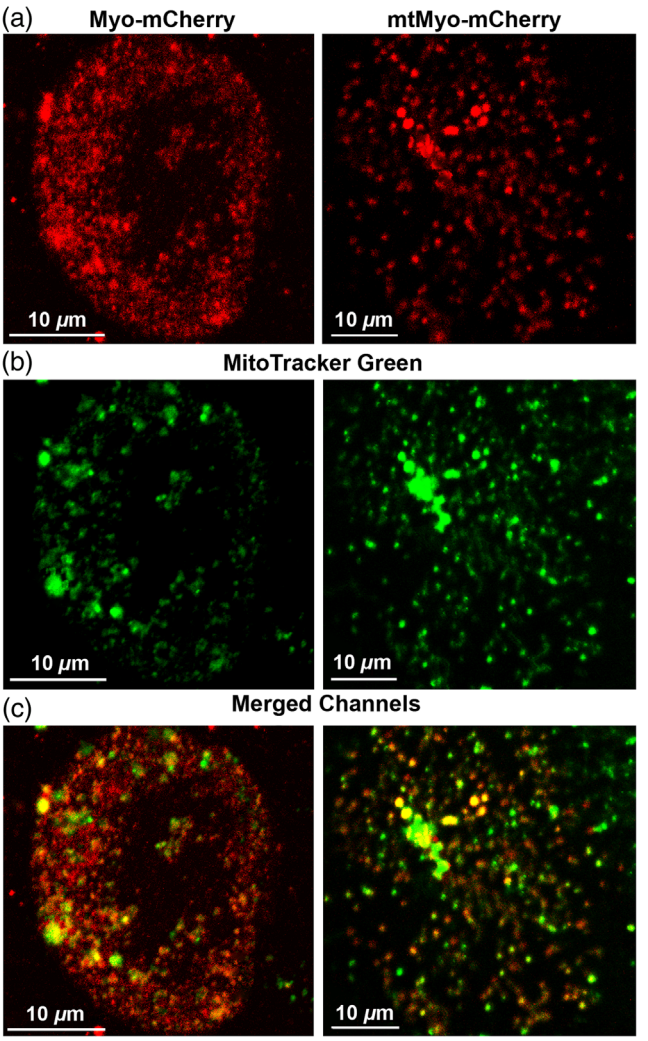

Fig. 2 Fluorescence images of A549 cells transfected with (a) Myo-mCherry and mtMyo-mCherry and stained with (b) MitoTracker Green. (c) Colocalization of the two channels of red (mCherry) and green (MitoTracker) fluorescence signals.

4.2 *Monitoring of the Intracellular Response of Myo-mCherry to Changes in the Imposed [O_2]*

Oxygen homeostasis is important for maintenance of the cells, tissues, and whole organisms. The intracellular [O_2] dynamically changes due to any imbalance in consumption and supply in response to the extracellular microenvironment and intracellular activity.[9] Changes in the intracellular [O_2] in response to different imposed external [O_2] was monitored by two-photon lifetime imaging of Myo-mCherry in transfected A549 cells. Table 1 presents the % O_2 (20%, 19%, 16%, 13%, 10%, 7%, 4%, 1%, and 0.5%) set at the gas mixer, and the corresponding O_2 partial pressure (pO_2) reached in the air, and in the culture media inside the miniature incubator during the experiments. OxyLite Pro 2 was used for the point measurements of the [O_2] in air and culture media. It is worth noting that the mitochondrial respiration creates an O_2 sink at the bottom of the culture dish, and thereby sets up an O_2 gradient through the culture medium. We also note that it is difficult to truly reach "0" mmHg in such a gas-exchange chamber and 0.6 ± 0.2 mmHg is the lowest [O_2] obtained by our system. This [O_2] might not correspond to full anoxia that may require over 24 h of complete equilibration in a hypoxic chamber.[34]

The pseudocolor mapping of the fluorescence lifetimes of Myo-mCherry in A549 cells is shown in Fig. 3(a) (first row), where red color indicates a shorter fluorescence lifetime with lower [O_2] and blue color indicates a longer lifetime with higher [O_2]. It is reported that mCherry has two microscopic states (a bright and a dim state), which leads to its biexponential fluorescence lifetime decay.[20] This behavior is also reflected by the Myo-mCherry probe, with a fluorescence lifetime decay that is adequately fit by a biexponential function. However, for determining lifetime changes as a function of extracellular [O_2], the amplitude-weighted average lifetime was used as the experimental readout. In Fig. 3(b), the solid dark blue, white, gray, and red lines in the lifetime pixel histograms show the average lifetime distribution at [O_2] of 20%, 10%, 4%, and 0.5%, respectively. Based on the fit of the pixel-based fluorescence intensity decay to Eq. (1), the average fluorescence lifetime of Myo-mCherry in the intracellular environment of A549 cell typically decreased from 1.27 to 0.94 ns by changing the external [O_2] from 20% to 0.5%. While a shallow decrease of the lifetime was monitored in response to the decrease of the external [O_2] from 20% to 10% (1.27 ns compared to 1.24 ns); a very steep decrease of the lifetime was observed in response to [O_2] decrease from 10% to 0.5% (1.24 ns compared to 0.94 ns). As shown in Table 2, the ratio between pre-exponential amplitudes in Eq. (1) was $C_2/C_1 = 0.59 \pm 0.16$ (two lifetimes, $\tau_1 = 0.58 \pm 0.11$ ns, $\tau_2 = 2.50 \pm 0.38$ ns) at $[O_2] = 20\%$, and $C_2/C_1 = 0.44 \pm 0.10$ (two lifetimes, $\tau_1 = 0.44 \pm 0.08$ ns, $\tau_2 = 2.20 \pm 0.21$ ns) at $[O_2] = 0.5\%$.

Mitochondria are the primary consumers of O_2 in cells due to oxidative phosphorylation, which is the primary metabolic pathway for adenosine triphosphate (ATP) and adenosine diphosphate (ADP) production.[6] Therefore, monitoring mitochondrial O_2 consumption level can be used as a means of understanding metabolic phenomena underlying physiological

Table 1 External [O_2] in the air and cell culture media inside the miniature incubator used for the fluorescence lifetime imaging of actively respiring cells. The values are presented with the standard deviation obtained from four measurements.

[O_2]	20%	19%	16%	13%	10%	7%	4%	1%	0.5%
Air (mmHg)	134.4 ± 3.5	132.0 ± 4.1	112.1 ± 6.1	94.4 ± 6.4	70.5 ± 1.3	50.1 ± 0.9	29.3 ± 2.5	8.3 ± 1.9	3.0 ± 0.5
Cell media (mmHg)	110.4 ± 7.2	108.1 ± 7.2	92.8 ± 11.1	86.9 ± 11.3	59.3 ± 11.2	36.5 ± 11.2	20.7 ± 5.9	5.6 ± 1.0	1.4 ± 0.5
Cell layer (mmHg)	89.5 ± 4.4	70.4 ± 4.8	56.5 ± 4.9	42.9 ± 6.1	33.3 ± 6.1	21.0 ± 7.5	10.3 ± 3.9	2.3 ± 0.8	0.6 ± 0.2
Control media (mmHg)	110 ± 4.8	108.8 ± 2.2	92.5 ± 3.4	89.5 ± 4.4	61.8 ± 3.4	37.6 ± 1.9	20.7 ± 2.0	5.9 ± 0.5	1.4 ± 0.4

Note: Cell media: The probe was inserted in the media ~1 mm below the top surface.
Cell layer: The bottom of Lab-Tek Petri dish, where the cells are adhered.
Control media: [O_2] in the media without the cells.

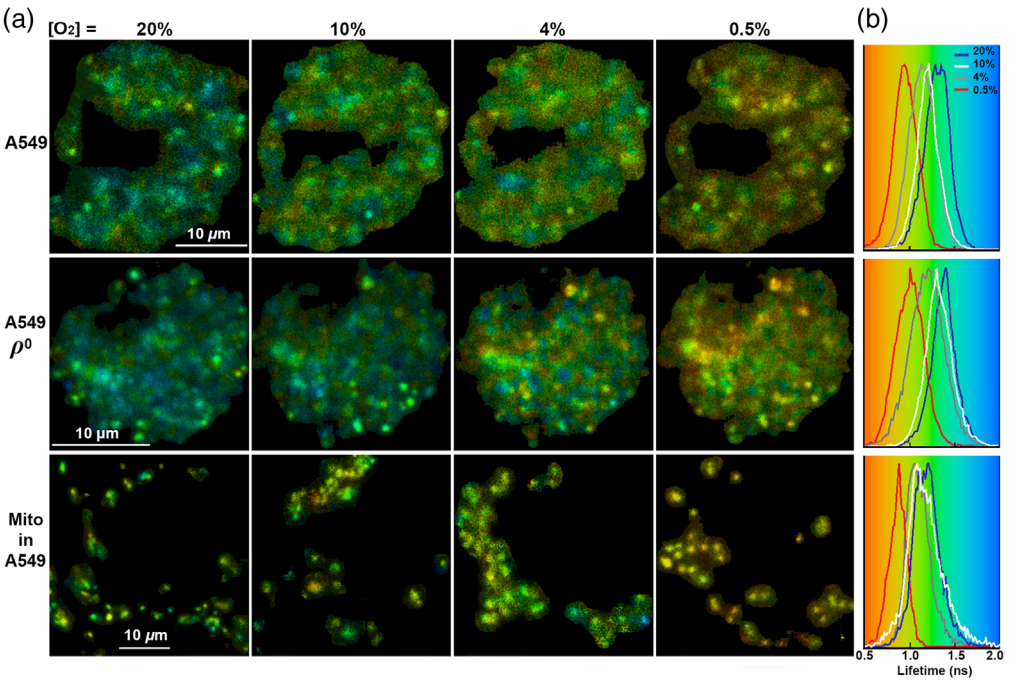

Fig. 3 (a) Pseudocolor mapping of Myo-mCherry fluorescence lifetime in the intracellular environment of A549 cells, A549 DNA-depleted ρ^0 cells, and A549 mitochondria (Mito) in response to 20%, 10%, 4%, and 0.5% external oxygen concentration ([O_2]) (see Table 1 for [O_2] in mmHg). (b) Fluorescence lifetime distribution histogram of Myo-mCherry; red indicates a shorter lifetime with smaller [O_2] and blue indicates a longer lifetime with higher [O_2]. The solid dark blue, white, gray, and red lines in (b) show the average lifetime peak at [O_2] of 20%, 10%, 4%, and 0.5%, respectively. The scale bars show 10 μm.

and pathological processes. The efficacy of our probe for indirect mapping and monitoring of the mitochondrial O_2 consumption by measuring [O_2] levels was evaluated in A549 cells. For this reason, the fluorescence lifetime of Myo-mCherry in A549 cells was compared to A549 mtDNA-depleted ρ^0 counterparts that are auxotrophic for pyruvate and uridine, and are incapable of aerobic respiration due to the lack of key respiratory chain components.[35] As shown in Fig. 3(a) (second row), A549 ρ^0 cells provided different lifetime images in response to external [O_2] variation compared to wt A549 cells. At the same imposed [O_2], A549 ρ^0 cells presented a longer average fluorescence lifetime for Myo-mCherry. The average lifetime of Myo-mCherry in the intracellular environment of A549 ρ^0 cells typically decreased from 1.34 to 0.98 ns by changing the external [O_2] from 20% (solid dark blue line in the lifetime pixel histograms) to 0.5% (solid red line in the lifetime pixel histograms) as shown in the second row in Fig. 3(b). We suggest that these longer lifetimes at moderate exogenous [O_2] are due to the lack of mitochondrial O_2 consumption in A549 ρ^0 cells leading to higher actual intracellular [O_2] as compared to respiring A549 cells. The ratio between pre-exponential amplitudes was $C_2/C_1 = 0.66 \pm 0.18$ (two lifetimes, $\tau_1 = 0.65 \pm 0.14$ ns, $\tau_2 = 2.58 \pm 0.30$ ns) at [O_2] = 20%, and $C_2/C_1 = 0.44 \pm 0.08$ (two lifetimes, $\tau_1 = 0.46 \pm 0.05$ ns, $\tau_2 = 2.37 \pm 0.21$ ns) at [O_2] = 0.5% for A549 ρ^0 cells (see Table 2).

Recent findings studying mitochondrial parameters other than respiratory rates (such as morphology and inner membrane potentials) suggest a significant heterogeneity between different cells in a population and among different mitochondria within the same cell.[9,36] As a result, the development of methodologies capable of measuring mitochondrial O_2 sinks with single cell resolution has become of interest. As shown in the third row

Table 2 Pre-exponential factors (C_1 and C_2) and their corresponding lifetimes (τ_1 and τ_2) in Eq. (1) obtained for the cells transfected with Myo-mCherry and mCherry alone as a control. The results have been shown for the lowest and highest imposed external [O_2].

	[O_2] (%)	τ_1 (ns)	τ_2 (ns)	C_1 (%)	C_2 (%)	C_2/C_1	τ_{Mean} (ns)
A549	0	0.44 ± 0.08	2.20 ± 0.21	70 ± 5	30 ± 5	0.44 ± 0.10	0.94 ± 0.06
	20	0.58 ± 0.11	2.50 ± 0.38	63 ± 6	36 ± 6	0.59 ± 0.16	1.27 ± 0.04
A549 ρ^0	0	0.46 ± 0.05	2.37 ± 0.21	70 ± 3	30 ± 3	0.44 ± 0.08	0.98 ± 0.05
	20	0.65 ± 0.14	2.58 ± 0.30	61 ± 6	39 ± 6	0.66 ± 0.18	1.34 ± 0.05
Mito-targeted	0	0.44 ± 0.06	2.19 ± 0.24	72 ± 6	29 ± 6	0.41 ± 0.14	0.94 ± 0.05
	20	0.52 ± 0.08	2.43 ± 0.30	66 ± 6	34 ± 6	0.53 ± 0.13	1.18 ± 0.04
Control	0	0.65 ± 0.07	2.79 ± 0.18	63 ± 2	37 ± 2	0.59 ± 0.05	1.34 ± 0.02
	20	0.59 ± 0.05	2.84 ± 0.30	62 ± 2	39 ± 2	0.63 ± 0.06	1.35 ± 0.06

Note: Mito-targeted: mitochondria-targeted in A549 cell.
Control: Cells transfected with mCherry only.

in Fig. 3, we further selectively monitored the mitochondrial [O_2] within A549 cells by adding a peptide to direct Myo-mCherry probe via the mitochondrial targeting sequence (mtMyo-mCherry). As shown in Fig. 3(b), at the same external [O_2], the average targeted mitochondrial [O_2] was seen to be lower than the [O_2] level averaged over the entire A549 and A549 ρ^0 cells. However, based on the statistical analyses conducted on a sample of 40 cells, A549 mitochondria-targeted influence on the intracellular O_2 consumption at "hypoxia" −0.5%—was not significantly different from those obtained for A549 cells. This allows us to state that the probe shows the same lowest lifetime value when fully deoxygenated, regardless of localization within the cell. In the active range, the average lifetime measured for mitochondria-targeted typically decreased from 1.18 to 0.94 ns by changing the external [O_2] from 20% (solid dark blue line in the lifetime histograms) to 0.5% (solid red line in the lifetime histograms), respectively. It is reasonable to expect lower [O_2] within and close to these active oxygen sinks even at higher imposed [O_2]. As shown in Table 2, the ratio between pre-exponential amplitudes was $C_2/C_1 = 0.53 \pm 0.13$ (two lifetimes, $\tau_1 = 0.52 \pm 0.08$ ns, $\tau_2 = 2.43 \pm 0.30$ ns) at $[O_2] = 20\%$, and $C_2/C_1 = 0.41 \pm 0.14$

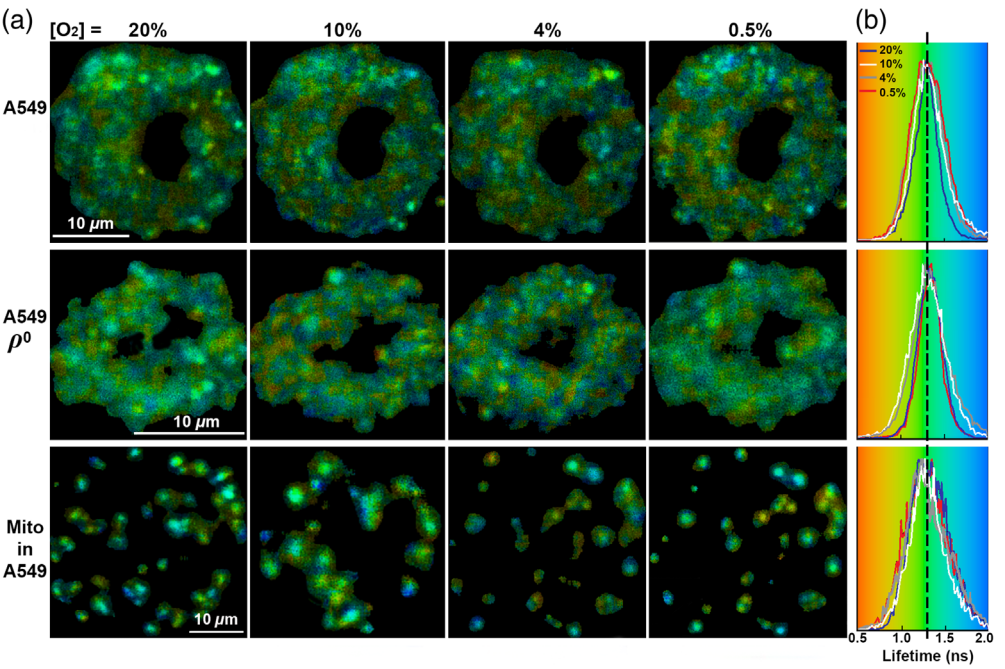

Fig. 4 (a) Fluorescence lifetime images of mCherry in the intracellular environment of A549 cells, A549 DNA-depleted ρ^0 cells, and A549 mitochondria (Mito); cells were exposed to 20%, 10%, 4%, and 0.5% external oxygen concentration ([O_2]) (see Table 1 for [O_2] in mmHg). (b) Fluorescence lifetime distribution histogram of mCherry; red indicates a shorter lifetime with smaller [O_2] and blue indicates a longer lifetime with higher [O_2]. The solid dark blue, white, gray, and red lines in (b) show the average lifetime peak at [O_2] of 20%, 10%, 4%, and 0.5%, respectively. Black dashed line compares the center of peak and the scale bars show 10 μm.

(two lifetimes, $\tau_1 = 0.44 \pm 0.06$ ns, $\tau_2 = 2.19 \pm 0.24$ ns) at $[O_2] = 0.5\%$ for A549 targeted mitochondria.

Control FLIM experiments were performed with A549, A549 ρ^0 cells as well as A549 mitochondria-targeted cells transfected with mCherry alone (the O_2-sensitive domain being absent) to examine the consistency of the lifetime values at different external $[O_2]$ [see Fig. 4(a)]. The mean fluorescence lifetime of mCherry averaged over the entire cell was measured to be (1.34 to 1.36) ± 0.06 ns in all experiments and, most importantly, was insensitive to the $[O_2]$ [see the center of peak specified with a dashed black line in Fig. 4(b)]. The lifetime value is presented with the standard deviation from 20 independent measurements. The ratio between pre-exponential amplitudes was calculated to be $C_2/C_1 = 0.63 \pm 0.06$, and the two lifetimes were $\tau_1 = 0.59 \pm 0.05$ ns, $\tau_1 = 2.84 \pm 0.30$ ns (see Table 2).

Except for mitochondria-targeted lifetime images, all other images shown in Figs. 3 and 4 are from the same A549 and A549 ρ^0 cells in the same field of view. We found it very difficult to track which mitochondria were measured at each step due to the motion of the organelle.

Myoglobin is made of a single polypeptide with only one heme group and hence is not capable of cooperative binding. The myoglobin-O_2 saturation curve is generally well described by a hyperbolic function[22,30] and it is reasonable to think that the addition of mCherry at the C-terminus of the protein, although it may alter the O_2-binding affinity, should not introduce a cooperative site. The average Myo-mCherry fluorescence lifetime increased in a hyperbolic manner in response to the increase in the $[O_2]$ imposed to A549 and A549 ρ^0 cells as well as to A549 mitochondria-targeted. Average intracellular lifetime of Myo-mCherry ($\tau([O_2])$) is well fit by Eq. (2). Figure 5(a) shows the average lifetime data versus external $[O_2]$ (in mmHg) measured by using OxyLite Pro. Whereas A549 ρ^0 cells do not consume oxygen and $[O_2]$ is assumed to remain about constant throughout the media, the mitochondrial respiration in A549 cells creates an oxygen sink at the bottom of the culture dish. Therefore, the lifetime values in A549 ρ^0 cells were correlated to $[O_2]$ measured in the control media. The lifetime values of A549 and A549 mitochondria-targeted were correlated to $[O_2]$ measured close to the cell layer, where the cells are adhered. The vertical error bars are the standard deviations of the fluorescence lifetime values obtained from 20 to 40 cells imaged in three to four independent experiments. The horizontal error bars are the standard deviations of the $[O_2]$ values measured from four independent measurements. The curves in this figure present the best hyperbolic fit to the data. Table 3 summarizes the fitting parameters and the goodness of fit, R^2.

To determine whether the observed differences in measured lifetime among A549, A549 ρ^0 cells, and A549 mitochondria-targeted are significant, statistical analyses were performed. Except for $[O_2]$ ~0.6 mmHg, Mann–Whitney tests showed a statistically significant difference between the lifetimes of each two independent groups in all possible pairwise combinations. In all combinations, the maximum p-value of the considered differences between the lifetime values at the same external $[O_2]$ was <0.003, which connotes statistical significance. The average lifetime of Myo-mCherry in A549 cells in response to external $[O_2]$ ~0.6 mmHg was not significantly different from that obtained for the A549 mitochondria-targeted. Due to the tight binding affinity of myoglobin itself, it is not

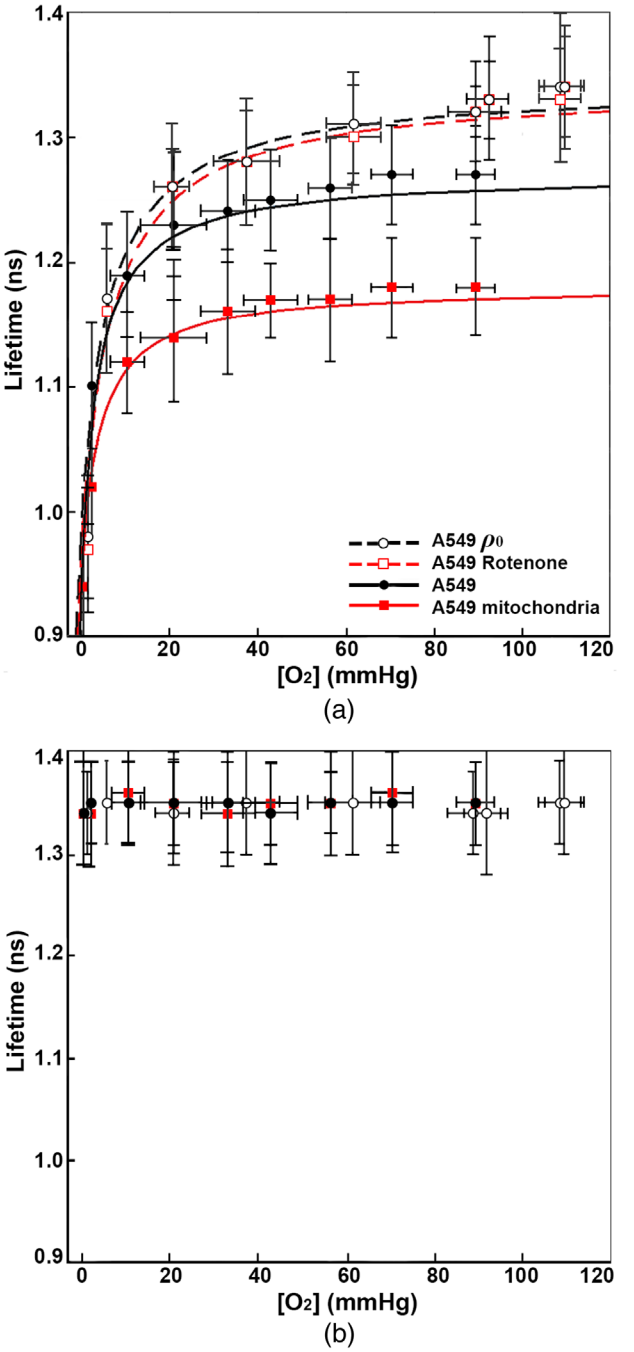

Fig. 5 (a) Average fluorescence lifetime of Myo-mCherry versus oxygen concentration ($[O_2]$) obtained from lifetime imaging of the mitochondria targeted protein (red-filled square) in A549 cells and the cytosolic distributed protein in A549 cells (black-filled circle), DNA-depleted A549 ρ^0 cells (empty circle) and A549 cells incubated with rotenone (empty square). Cells were exposed to external $[O_2]$ from 20% to 0.5%; x axis reports the $[O_2]$ in the media measured by OxyLite probe (see Table 1 for the relationship between $[O_2]$ in % and $[O_2]$ in mmHg). The data are shown with the best hyperbolic fit [Eq. (2)] and the fitting parameters and goodness of fit, R^2, have been shown in Table 3. (b) Average fluorescence lifetime of mCherry versus $[O_2]$ in mitochondria-targeted in A549 cells and the cytosolic distributed protein in A549 and, A549 ρ^0 cells [same legend as (a)]. Vertical and horizontal error bars in (a) and (b) represent the standard deviation.

Table 3 Fitting parameters of the hyperbolic model in Eq. (2) extracted from average Myo-mCherry lifetime values as a function of $[O_2]$ (in mmHg). The data and the fitting curves have been shown in Fig. 5(a).

	τ_{max}	τ_{min}	a	R^2
A549 ρ^0	1.34	0.98	5.97	0.95
A549 rotenone	1.34	0.97	6.79	0.95
A549	1.27	0.94	3.68	0.96
A549 mitochondria targeted	1.18	0.94	3.93	0.97

unreasonable to hypothesize that the convergence of all observations for lifetime observed (at 0.5% imposed oxygen level) could be explained by considering that at such low $[O_2]$ the rates of consumption have less influence. Further, this convergence at minimal oxygen strongly suggests that other modifiers of average lifetime are small compared to the primary oxygen-sensing response.

We tested whether Myo-mCherry has the same lifetimes versus $[O_2]$ in A549 ρ^0 and A549 cells exposed to the mitochondrial complex I inhibitor Rotenone. Incubation of A549 cells with 500 nM rotenone for 1 h caused a significant inhibition of mitochondrial electron transport, as inferred by a significant increase in Myo-mCherry lifetimes [see Fig. 5(a)] that corresponds to overall higher cytoplasmic $[O_2]$ compared to untreated cells. There was no statistically significant difference between the lifetimes obtained for A549 ρ^0 and A549 cells treated with rotenone. All these FLIM and statistical analyses confirm that our probe can report the changes of the intracellular $[O_2]$ and the mitochondrial contribution to cellular O_2 consumption in response to different external $[O_2]$.

As shown in Fig. 5(b), mCherry lifetime is insensitive to the intracellular $[O_2]$ level. The lifetime of mCherry at each $[O_2]$ has been shown with error bars that are the standard deviations calculated for 20 cells. Mann–Whitney tests did not show any statistically significant difference between the lifetimes of each two independent groups (at different environmental $[O_2]$) in all possible pairwise combinations. This allows us to confirm that (on average) intracellular environmental variables, such as refractive index or temperature, have a negligible effect on the fluorescence lifetime of mCherry compared to the effect exerted by the $[O_2]$-sensing domain in the Myo-mCherry construct.

5 Conclusion

The aim of the present study was to develop a noninvasive and accurate method for sensing intracellular $[O_2]$ in living cells based on lifetime measurements for a reporter that can be easily delivered with transfection methods, and eventually could be integrated in the genome of cell lines, or organisms. We therefore designed a FLIM-FRET-based probe, Myo-mCherry, that can be expressed in cells and tissue without disruption (e.g., cells transfected with Myo-mCherry did not show any sign of cytotoxicity up to three days after the transfection). The O_2-sensing efficacy of Myo-mCherry in living A549 cells, and their electron-chain DNA-depleted counterpart ρ^0 cells was evaluated. We demonstrated that lifetime imaging of Myo-mCherry is capable of reliably monitoring single cell $[O_2]$ level, responding to mitochondrial contributions to intracellular O_2 consumption in the expected manner, and mapping intercell variability in response to the changes in external $[O_2]$. When Myo-mCherry was targeted to mitochondria via the mitochondrial-targeting sequence, mtMyo-mCherry monitored mitochondrial $[O_2]$ level, and uncovered heterogeneity in consumption patterns within the same cells. In contrast to the available methods that provide $[O_2]$ based on the measurements of fluorescence intensity, our FLIM-FRET-based probe produces results that are independent of the probe concentration. Moreover, Myo-mCherry is compatible with the deepest forms of multiphoton FLIM inside tissue, due to its compatibility with two-photon excitation and its emission in the red part of the visible spectrum. The use of longer excitation wavelength results in reduced scatter losses and damage to tissue.[37,38] Due to the short fluorescence lifetime of Myo-mCherry, our O_2-sensing system is compatible with the highest scan rates available. We used TCSPC collection for this data, but high scan rate FLIM should obtain the same information. By sacrificing some spatial resolution and/or employing a higher photon budget, we estimate it may be possible to collect enough photons in a high rate (~10 MHz) stream for TCSPC or for analog digitization in "fast FLIM" modules to collect $[O_2]$ maps at 1-s frame rates or faster. This circumvents the problem of long acquisition time encountered in other techniques such as PLIM, which complicates live-cell imaging (due to dynamic rearrangement at the subcellular level or phototoxicity) and *in vivo* studies (due to body motion or heartbeat during imaging).

In conclusion, we have successfully demonstrated the feasibility of real-time noninvasive imaging of intracellular and mitochondrial $[O_2]$ level, a development that will add knowledge of physiological and pathological O_2 metabolism on a single-cell basis. We have already shown subcellular resolution (mitochondrial) data and we foresee the compatibility of the probe with superresolved FLIM, when combined with stimulated emission depletion. The mapping of the perimitochondrial $[O_2]$ gradients is essential for evaluation of their dysfunction since ATP- and ADP-dependent O_2 consumption directly reflects oxidative phosphorylation or coupled respiration.[3,39] This $[O_2]$ probe may also provide new directions for detection and therapeutic strategies targeted to mitochondria for treatment of diseases caused by dysfunction of these organelles, which pose severe and costly threats to public health.

6 Appendix

6.1 *Single Pixel Intracellular Lifetime Decay Curves of mCherry and Myo-mCherry*

Double-exponential decays of mCherry and Myo-mCherry in the intracellular environment are shown in Fig. 6. The molecules were excited by a very short laser pulse and the decay of fluorescence intensity was measured by TCSPC. Whereas intensity decays of mCherry [see Fig. 6(a)] remained about the same at the external $[O_2]$ of 20%, 10%, 4%, and 0.5%, the decays of Myo-mCherry clearly changed with decreasing external $[O_2]$.

6.2 *Resonance Energy Transfer between mCherry and Myoglobin*

The working principle of the Myo-mCherry construct is based on FRET, where the mCherry acts as a fluorescent donor and myoglobin is the dark acceptor. A comparison of the emission

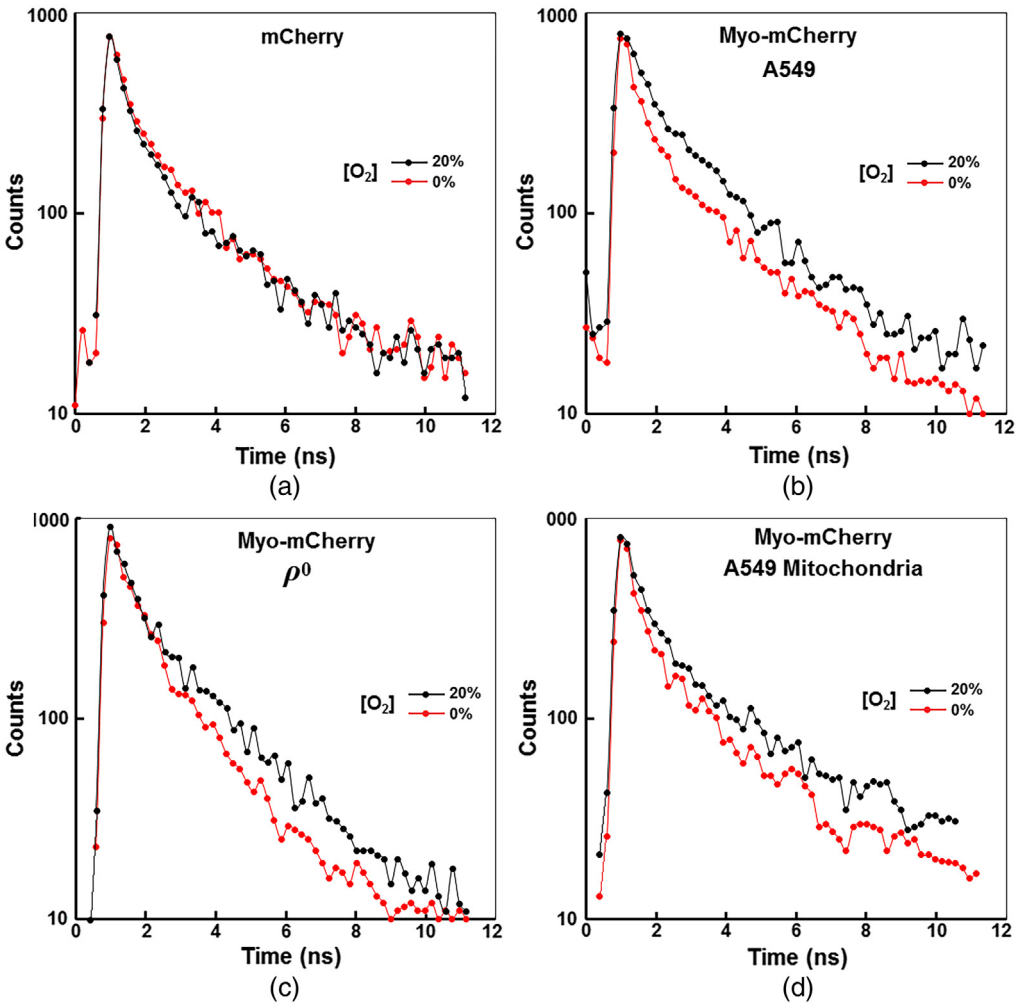

Fig. 6 Representative single (binned) pixel decay data, as a function of oxygen concentration, showing double exponential trend of: (a) mCherry in the intracellular environment of A549 cells, (b) Myo-mCherry in A549 cells, (c) Myo-mCherry in A549 mitochondrial DNA-depleted (mtDNA) ρ^0 counterparts, and (d) Myo-mCherry in A549 mitochondria-targeted at 20%, 10%, 4%, and 0% external oxygen concentration ($[O_2]$).

spectra of mCherry and Myo-mCherry measured directly in A549 cells is shown in Fig. 7.

The changes in spectral features of myoglobin upon O_2 binding and unbinding cause the amount of energy transferred from the fluorescent protein to vary depending on whether myoglobin is in the oxygenated (oxy) or deoxygenated (deoxy) state. The spectral overlap $J(\lambda)$ can be calculated as

$$J(\lambda) = \frac{\int_0^\infty F_D(\lambda)\varepsilon_A(\lambda)\lambda^4 \mathrm{d}\lambda}{\int_0^\infty F_D(\lambda)\mathrm{d}\lambda} \tag{4}$$

where $F_D(\lambda)$ is the fluorescence intensity emission of the donor molecule, ε_A is the extinction coefficient of the acceptor, and λ is the wavelength. Using $J(\lambda)$, the Förster radius can be calculated as[40]

$$R_0 = 0.211[\kappa^2 n^{-4} Q_D J(\lambda)]^{1/6}, \tag{5}$$

where κ is the factor that accounts for the relative orientation and position of the donor and acceptor dipoles,[41] n is the refractive index of the media, and Q_D is the QY of the energy donor. The transfer efficiency can then be derived as[40,42]

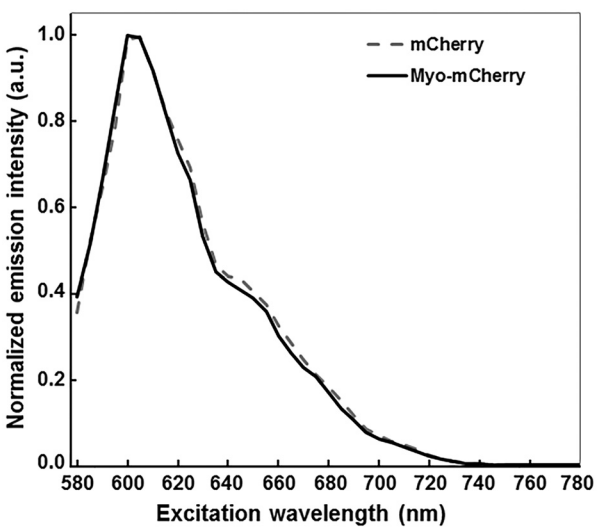

Fig. 7 Emission spectra of mCherry (dashed gray line) and Myo-mCherry (solid black line) in A549 cells. Each spectrum is the average of spectra collected from five cells.

$$E(r) = \frac{1}{1 + \frac{r^6}{R_0^6}}, \tag{6}$$

where r is the distance between the two molecules undergoing energy transfer. The relationship between energy transfer efficiency and lifetime of the donor is derived as[40]

$$E = 1 - \frac{\tau_{DA}}{\tau_D}, \tag{7}$$

where τ_D is the lifetime of the donor alone, and τ_{DA} is the lifetime of the donor when the acceptor molecule is present in its proximity.

In our calculations, the spectral data for myoglobin were obtained from Ref. 22, and the extinction coefficients were used as reported in Ref. 23: $\lambda = 556$ nm, $\varepsilon = 11.8$ mM^{-1} cm^{-1} for deoxy and $\lambda = 543$ or 581 nm and $\varepsilon = 13.6$ or 14.6 mM^{-1} cm^{-1} for oxy. The emission spectrum for mCherry was taken as the average of the measurements performed on A549 cells transfected with pmCherry (see Fig. 7), and the spectral data were obtained from Ref. 21: $\lambda_{exc} = 587$ nm, $\varepsilon_{587\text{ nm}} = 72$ mM^{-1} cm^{-1}, and QY $= 0.22$. The average lifetime of mCherry was taken as the average of the measurements performed on A549 cells transfected with pmCherry: $\tau = 1.34$ ns. By using these parameters, the values of R_0 between mCherry and myoglobin were calculated to be 2.9 and 3.4 nm in the oxy state and in the deoxy state, respectively [see Fig. 1(b)]. The refractive index for an aqueous solution, $n = 1.333$, and the orientation factor for random static orientation, $\kappa^2 \approx (2/3) \times (1 - \langle E \rangle) = 0.507$, was used in our calculations; in our case $\langle E \rangle \sim 0.24$, and 0.507 only shows the rough correspondence of FRET with expectations.[43]

There are no structural data available for the Myo-mCherry construct, thus any estimate of the distance between the two chromophores is assumed to be a first approximation. Here, the available structures from the PDB for myoglobin (PDB entry 1MBO) and mCherry (PDB entry 2H5Q) were used to measure the intraprotein distances between each chromophore and the point where the two proteins are connected. The distance between the iron in the heme and the C-term of myoglobin is estimated to be ~2.6 nm and the distance between the N-term and the chromophore in mCherry is ~1.4 nm. If these chromophore-connection vectors are nearly collinear, a 4-nm distance can be assumed for further calculations. The energy transfer efficiency for the Myo-mCherry construct either in the oxy or the deoxy state are presented in the main text, Fig. 1(c). Using the information outlined above, the lifetimes based on the theoretical energy transfer rates $E_{oxy}(r = 4\text{ nm}) = 0.14$ and $E_{deoxy}(r = 4\text{ nm}) = 0.25$ is expected to be $\tau_{\text{Myo-mCherry}} = 1.16$ and 1.01 ns, respectively.

The actual lifetime measured for the two forms in living cells show that the energy transfer between mCherry and myoglobin in the oxy form is lower than predicted (measured $\tau_{\text{Myo-mCherry}} = 1.34$ ns in A549 ρ^0 cells), whereas a higher than predicted rate is observed for the deoxy form (measured $\tau_{\text{Myo-mCherry}} = 0.98$ ns in A549 ρ^0 cells). These minor differences could most likely be attributable to $\kappa^2 \neq 0.507$ (preferential conformations assumed by the two proteins), but noncollinearity of the absorption dipoles of oxy and deoxy myoglobin or influence of the cellular microenvironment on the absorption and emission spectra of myoglobin or mCherry could also be present. Although a detailed characterization of these biophysical properties would be advantageous to understand and improve future designs, it is beyond the scope of this work and it will be presented elsewhere.

6.3 *Derivation of the Hyperbolic Function Used to Fit Lifetime Versus Partial Pressure of Oxygen (p_{O_2}po)*

The binding of O_2 to globins is generally described by the Hill equation,[22] which describes saturations of the binding sites as a function of partial pressure of oxygen (p_{O_2}):

$$Y = \frac{(p_{O_2})^n}{(p_{O_2})^n + (P_{50})^n}, \tag{8}$$

where Y is the fraction of protein bound to O_2, P_{50} is the partial pressure of oxygen at $Y = 0.5$, and n is the binding cooperativity index. For myoglobin, the value of n has been established to be 1, and thus the equation simplifies to a hyperbolic function.[22] In this work, it is assumed that the addition of mCherry to myoglobin does not change its binding behavior with O_2. It is possible, although not yet verified, that the binding affinity (P_{50}) might differ from the wild-type protein. However, this will be discussed elsewhere in more detail. To describe the data presented in Fig. 5, it was noticed that a hyperbolic fit was satisfactory: the physical meaning of this can be traced to the behavior of myoglobin. The average lifetime observed in cells at each [O_2] can be thought of as the sum of contributions from the lifetime of each of the species, weighted by their molar fraction. This can be written as

$$\tau_{avg}(p_{O_2}) = \chi_{oxy}\tau_{oxy} + (1 - \chi_{oxy})\tau_{deoxy}, \tag{9}$$

where $\tau_{avg}(p_{O_2})$ is the average lifetime measured across a cell (or average of several cells) at a particular p_{O_2}; χ_{oxy} is the molar fraction of oxy Myo-mCherry in those particular conditions; τ_{oxy} and τ_{deoxy} are the Myo-mCherry lifetimes in fully oxy and fully deoxy states, respectively. The parameter χ_{oxy} is equivalent to the fraction Y described already, and thus the equation can be rewritten and rearranged to yield:

$$\tau_{avg}(p_{O_2}) = (\tau_{oxy} - \tau_{deoxy})\frac{p_{O_2}}{p_{O_2} + a} + \tau_{deoxy}. \tag{10}$$

However, P_{50} was substituted with the parameter a instead. Unlike experiments in solution *in vitro*, here the protein is immersed in an out of equilibrium environment, the cytoplasm, where O_2 is constantly consumed by metabolic reactions and thus its concentration inside the cell might be different than the concentration measured inside the media during the experiments.

The primary intention of this work is to present a proof of principle of how the newly developed Myo-mCherry oxygen probe can be used to monitor [O_2] inside living cells. The layout of Fig. 5 is meant to highlight the hyperbolic response of the lifetime of Myo-mCherry as a function of [O_2], and its agreement with the model presented above. For biosensing applications, it is useful to present the readout of the sensor as a function of analyte concentration in a straightforward format. Thanks to one of the anonymous reviewers, we found that a logarithmic x axis allows to present the data emphasizing the large changes in lifetime values occurring at low [O_2].

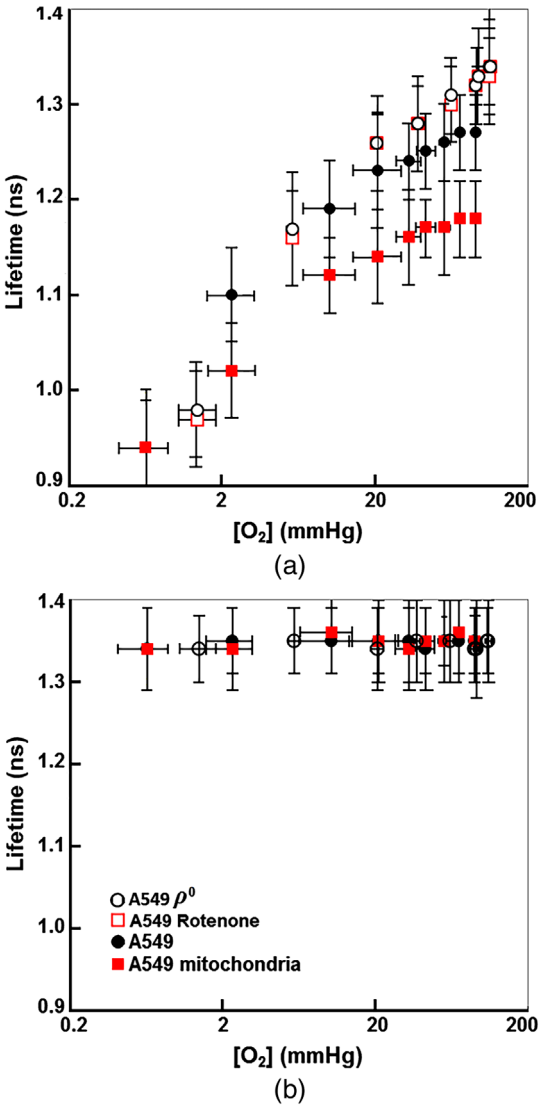

Fig. 8 Alternative representation of the data shown in Fig. 5, with the *x* axis scale in logarithmic unit. For details, refer to the main text of the article and the caption of Fig. 5.

For completeness, we show above in Fig. 8 this alternative representation.

Disclosures

The authors have no relevant financial interests in this article and no potential conflicts of interest to disclose.

Acknowledgments

We would like to acknowledge the Light Microscopy Core at the National Heart, Lung, and Blood Institute (NHLBI) for the use of their confocal microscopes for colocalization and spectral imaging. Special thanks to Dr. Christian Combs, Director of Light Microscopy Core, for helpful discussions and advice on colocalization imaging and analyses. We are also thankful to Dr. Timothy C. Zhu and his group at the Department of Radiation Oncology, University of Pennsylvania for providing us with OxyLite Pro 2 Channel monitor. This work was supported by the Intramural Research Program of NHLBI, and in part by funds from the Eunice Kennedy Shriver National Institute of Child Health and Human Development (NICHD), National Institutes of Health (NIH).

Portions of this work have previously appeared in abstract and presentation form in R. Penjweini et al., "Non-invasive monitoring of mitochondrial oxygen consumption and intracellular distribution of [O_2]," *Biophysical Journal* **114**(3), 20a (2018) and A. Andreoni et al., "A breath of fresh air: a genetically encoded O_2 probe for direct mapping and quantification of oxygenation levels in cells via fluorescence lifetime imaging," *Biophysical Journal* **114**(3), 359a (2018).

References

1. L. A. Pham-Huy, H. He, and C. Pham-Huy, "Free radicals, antioxidants in disease and health," *Int. J. Biomed. Sci.* **4**(2), 89–96 (2008).
2. A. V. Zhdanov et al., "Monitoring of cell oxygenation and responses to metabolic stimulation by intracellular oxygen sensing technique," *Integr. Biol.* **2**(9), 443–451 (2010).
3. F. A. Harm et al., "Non-invasive monitoring of mitochondrial oxygenation and respiration in critical illness using a novel technique," *Crit. Care* **19**, 343 (2015).
4. R. Penjweini et al., "Investigating the impact of oxygen concentration and blood flow variation on photodynamic therapy," *Proc. SPIE* **9694**, 96940L (2016).
5. M. M. Kim et al., "Determination of the low concentration correction in the macroscopic singlet oxygen model for PDT," *Proc. SPIE* **9694**, 96940D (2016).
6. G. Solaini et al., "Hypoxia and mitochondrial oxidative metabolism," *Biochim. Biophys. Acta* **1797**(6–7), 1171–1177 (2010).
7. M. Robiolio, W. L. Rumsey, and D. F. Wilson, "Oxygen diffusion and mitochondrial respiration in neuroblastoma cells," *Am. J. Physiol.* **256**, C1207–C1213 (1989).
8. W. I. Sivitz and M. A. Yorek, "Mitochondrial dysfunction in diabetes: from molecular mechanisms to functional significance and therapeutic opportunities," *Antioxid. Redox Signaling* **12**(4), 537–577 (2010).
9. H. Kurokawa et al., "High resolution imaging of intracellular oxygen concentration by phosphorescence lifetime," *Sci. Rep.* **5**, 10657 (2015).
10. R. I. Dmitriev and D. B. Papkovsky, "Optical probes and techniques for O_2 measurement in live cells and tissue," *Cell Mol. Life Sci.* **69**(12), 2025–2039 (2012).
11. Y. Zhang et al., "Magnetic resonance imaging of vascular oxygenation changes during hyperoxia and carbogen challenges in the human retina," *Invest. Ophthalmol. Visual Sci.* **52**(1), 286–291 (2011).
12. D. Lloyd et al., "Intracellular oxygen: similar results from two methods of measurement using phosphorescent nanoparticles," *J. Innovative Opt. Health Sci.* **7**(2), 1350041 (2014).
13. D. Kessel, "Effects of photoactivated porphyrins at the cell surface of leukemia L1210 cells," *Biochemistry* **16**(15), 3443–3449 (1977).
14. C. F. Williams et al., "Evaluation of two novel methods for assessing intracellular oxygen," *Meas. Sci. Technol.* **23**(8), 084005 (2012).
15. T. Yoshihara et al., "Intracellular and in vivo oxygen sensing using phosphorescent Ir(III) complexes with a modified acetylacetonato ligand," *Anal. Chem.* **87**(5), 2710–2717 (2015).
16. R. B. Thompson and M. W. Patchan, "Fluorescence lifetime-based biosensing of zinc: origin of the broad dynamic range," *J. Fluoresc.* **5**(2), 123–130 (1995).
17. N. C. Shaner et al., "Improved monomeric red, orange and yellow fluorescent proteins derived from Discosoma sp. red fluorescent protein," *Nat. Biotechnol.* **22**(12), 1567–1572 (2004).
18. R. M. Hoffman, "The multiple uses of fluorescent proteins to visualize cancer in vivo," *Nat. Rev. Cancer* **5**(10), 796–806 (2005).
19. O. Thoumine et al., "Probing the dynamics of protein-protein interactions at neuronal contacts by optical imaging," *Chem. Rev.* **108**(5), 1565–1587 (2008).
20. B. Wu, Y. Chen, and J. D. Muller, "Fluorescence fluctuation spectroscopy of mCherry in living cells," *Biophys. J.* **96**(6), 2391–2404 (2009).
21. N. C. Shaner, P. A. Steinbach, and R. Y. Tsien, "A guide to choosing fluorescent proteins," *Nat. Methods* **2**(12), 905–909 (2005).

22. K. A. Schenkman et al., "Myoglobin oxygen dissociation by multiwavelength spectroscopy," *J. Appl. Physiol.* (1985) **82**(1), 86–92 (1997).
23. E. Antonini and M. Brunori, *Hemoglobin and Myoglobin in Their Reactions with Ligands*, North-Holland Publications Co., Amsterdam (1971).
24. Q. Sun et al., "Mechanism of two-photon excited hemoglobin fluorescence emission," *J. Biomed. Opt.* **20**(10), 105014 (2015).
25. S. S. Vogel et al., "The impact of heterogeneity and dark acceptor states on FRET: implications for using fluorescent protein donors and acceptors," *PLoS One* **7**(11), e49593 (2012).
26. B. A. Springer and S. G. Sligar, "High-level expression of sperm whale myoglobin in Escherichia coli," *Proc. Natl. Acad. Sci. U. S. A.* **84**(24), 8961–8965 (1987).
27. X. Chen, J. L. Zaro, and W. C. Shen, "Fusion protein linkers: property, design and functionality," *Adv. Drug Delivery Rev.* **65**(10), 1357–1369 (2013).
28. G. Han et al., "The mitochondrial complex I inhibitor rotenone induces endoplasmic reticulum stress and activation of GSK-3beta in cultured rat retinal cells," *Invest. Ophthalmol. Visual Sci.* **55**(9), 5616–28 (2014).
29. W. Becker, *The bh TCSPC Handbook*, 7th ed., Becker & Hickl GmbH, Berlin, Germany (2017).
30. A. Seiyama, "Virtual cooperativity in myoglobin oxygen saturation curve in skeletal muscle in vivo," *Dyn. Med.* **5**, 3 (2006).
31. S. Bolte and F. P. Cordelières, "A guided tour into subcellular colocalization analysis in light microscopy," *J. Microsc.* **224**(3), 213–232 (2006).
32. E. M. M. Manders, F. J. Verbeek, and J. A. Aten, "Measurement of co-localization of objects in dual-colour confocal images," *J. Microsc.* **169**(3), 375–382 (1993).
33. M. D. Brand and D. G. Nicholls, "Assessing mitochondrial dysfunction in cells," *Biochem. J.* **435**(2), 297–312 (2011).
34. T. L. Place, F. E. Domann, and A. J. Case, "Limitations of oxygen delivery to cells in culture: an underappreciated problem in basic and translational research," *Free Radical Biol. Med.* **113**, 311–322 (2017).
35. D. Magda et al., "mtDNA depletion confers specific gene expression profiles in human cells grown in culture and in xenograft," *BMC Genomics* **9**, 521 (2008).
36. C. S. Santos, A. J. Kowaltowski, and M. Bertotti, "Single cell oxygen mapping (SCOM) by scanning electrochemical microscopy uncovers heterogeneous intracellular oxygen consumption," *Sci. Rep.* **7**(1), 11428 (2017).
37. H. Ehsani et al., "Alteration of optical and morphological properties of polycarbonate illuminated by visible/IR laser beams," *J. Eur. Opt. Soc.* **5**, 100325 (2010).
38. C. Ash et al., "Effect of wavelength and beam width on penetration in light-tissue interaction using computational methods," *Lasers Med. Sci.* **32**(8), 1909–1918 (2017).
39. M. L. Hartman et al., "Relation of mitochondrial oxygen consumption in peripheral blood mononuclear cells to vascular function in type 2 diabetes mellitus," *Vasc. Med.* **19**(1), 67–74 (2014).
40. J. R. Lakowicz, *Principles of Fluorescence Spectroscopy*, 2nd ed., Kluwer Academic/Plenum, New York (1999).
41. R. E. Dale and J. Eisinger, "Intramolecular distances determined by energy transfer. Dependence on orientational freedom of donor and acceptor," *Biopolymers* **13**(8), 1573–1605 (1974).
42. T. H. Forster, "Intermolecular energy migration and fluorescence," *Ann. Phys.* **2**, 55–75 (1948).
43. S. S. Vogel, B. W. van der Meer, and P. S. Blank, "Estimating the distance separating fluorescent protein FRET pairs," *Methods* **66**(2), 131–138 (2014).

Rozhin Penjweini received her PhD in physics from the University of Vienna, Austria, in 2012. Currently, she is a postdoctoral fellow at NHLBI, NIH. Her current research interest is the monitoring of the intracellular and interstitial oxygenation and metabolism by using fluorescence lifetime imaging and super-resolution microscopy. She also has experience in various *in vivo* explicit photodynamic therapy techniques as well as fluorescence microscopy for studying the structure, transport, and stability of nanomedicines.

Alessio Andreoni received his PhD in biochemistry and biophysics from Leiden University, The Netherlands, in 2012, where he worked on single-molecule fluorescence studies of redox proteins and enzymes. Currently, he is a postdoctoral fellow at NHLBI, NIH. His current research interest is in the development and use of fluorescence-based biosensors and methods for the detection of biologically relevant metabolites. He has also experience in protein biochemistry, fluorescence spectroscopy, DNA nanotechnology, and microscopy applied to biological sensing.

Tilman Rosales received his PhD in chemical physics from the University of Maryland, College Park. He was a postdoctoral fellow at NHLBI, NIH from 2010 to 2016, where he worked on the Myo-mCherry biochemistry, and lifetime imaging for intracellular oxygen sensing. Currently, he is a medical student at Wayne State University School of Medicine.

Jeonghan Kim received his PhD in cell biology from Korea University, South Korea, in 2013. Currently, he is a postdoctoral fellow in the NHLBI, NIH. His research interests include functions of mitochondria in aging, inflammation and metabolic disease.

Michael D. Brenner graduated from the Department of Chemistry at the University of Illinois at Urbana-Champaign in 2013 (PhD), where he performed biochemistry within the Department of Physics. His work on applying single-molecule FRET techniques to transcription regulation and optical tweezers of proteins led him to postdoctoral fellowships at NIH and Oxford University. His research interests include biosensors, protein engineering, mechanotransduction, the extracellular matrix and the lysosomal-derived 'secretome,' lipid trafficking and evolutionary immunology.

Dan L. Sackett received his PhD in molecular and cellular biology from Brown University. His work has focused on cell division and microtubule biochemistry and biophysics, first at the National Institute of Arthritis, Diabetes, and Digestive and Kidney Diseases, NIH. His work continued at NCI until in 1999 he joined the Program in Physical Biology at NICHD. Currently, he is senior researcher in the Division of Basic and Translational Biophysics, NICHD, NIH, where his research focuses on biochemistry and pharmacology of tubulin, and biophysics of microtubules.

Jay H. Chung received his MD and PhD degrees from Harvard Medical School in 1988, where he specialized in molecular genetics. Currently, he is the chief of the Laboratory of Obesity and Aging Research at the NHLBI in the NIH. His group uses animal and tissue culture cell models to study mitochondrial function, energy metabolism and aging.

Jay R. Knutson received his PhD from the University of Minnesota in 1978. Currently, he is the chief of the Laboratory for Advanced Microscopy and Biophotonics at the NHLBI in NIH. This laboratory focuses on developing and exploiting new optical devices, techniques and reagents for biomedicine, particularly those employing ultrafast lasers, such as FLIM, CARS, STED (STAQ), and FFS.